

## Supplementary Information

### **Microscopic manipulation of ferroelectric domains in SnSe monolayers at room temperature**

Kai Chang<sup>1,\*†</sup>, Felix Küster<sup>1</sup>, Brandon J. Miller<sup>2</sup>, Jing-Rong Ji<sup>1</sup>, Jia-Lu Zhang<sup>1</sup>, Paolo Sessi<sup>1</sup>, Salvador Barraza-Lopez<sup>2</sup> & Stuart S. P. Parkin<sup>1,\*</sup>

1. Max Planck Institute of Microstructure Physics, Weinberg 2, Halle 06120, Germany

2. Department of Physics, University of Arkansas, Fayetteville, Arkansas 72701, USA

\* (K.C.) changkai@baqis.ac.cn; (S.S.P.P.) stuart.parkin@mpi-halle.mpg.de

† Current address: Beijing Academy of Quantum Information Sciences, Beijing 100193, China

This document contains

Supplementary Figures S1-S11;

A supplementary video showing the consecutive motion of a domain wall.

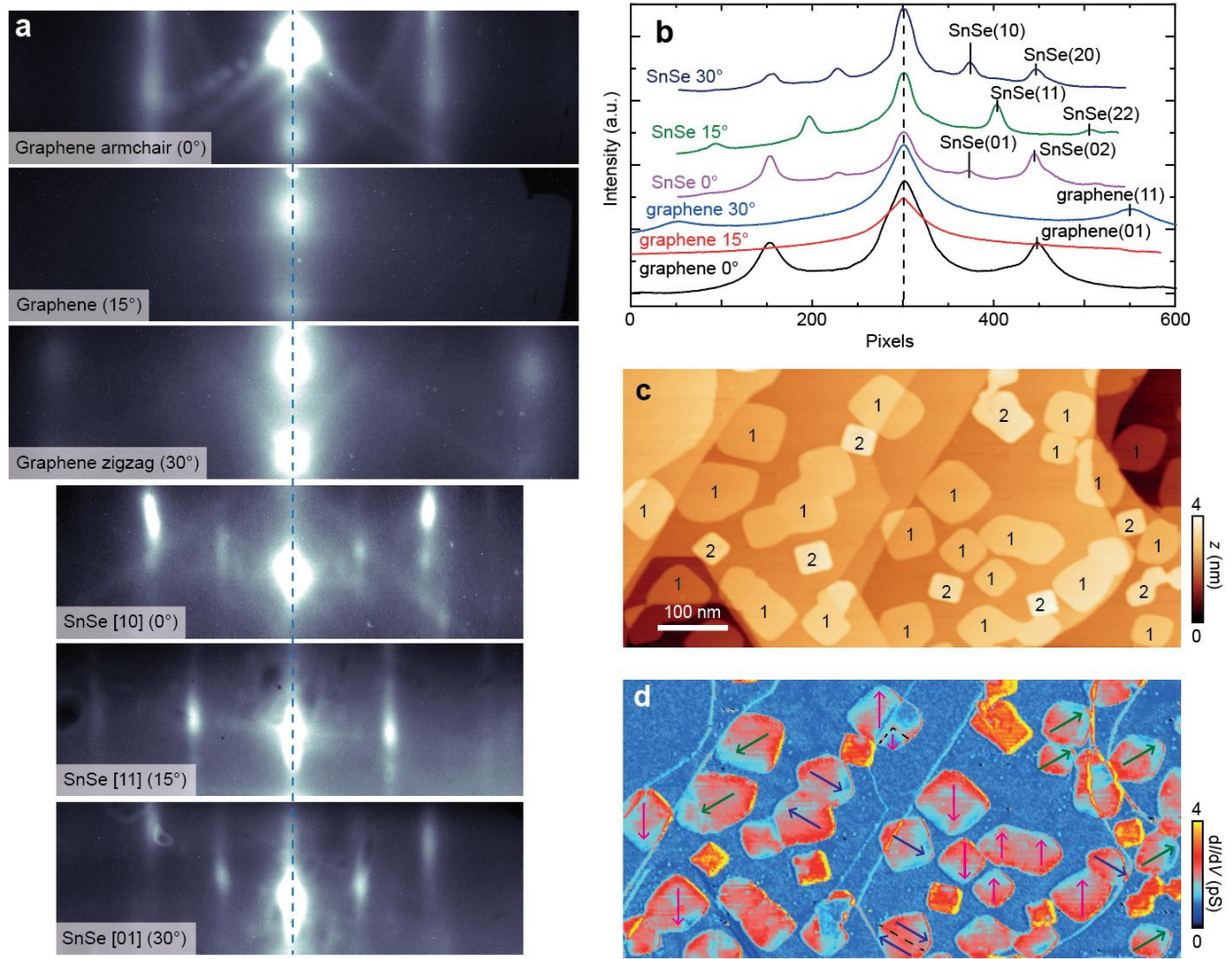


**Figure S1 | Experimental evidence of highly oriented growth.** **a**, RHEED patterns of a graphene substrate and SnSe plates grown on it (the average thickness is 5 MLs, in order to enhance the brightness of SnSe stripes). The incidence directions of electron beams are indicated in each panel, as well as the absolute azimuthal angle. **b**, Integrated RHEED intensity profiles extracted from **a**. The profiles are vertically shifted for clarity. The attributions of Bragg peaks are labeled. Similar RHEED patterns of SnSe appear along the zigzag (0°) and armchair (30°) directions of the graphene substrate, since the difference between the lattice constants along the [10] and [01] directions of SnSe ML is smaller than 0.1 Å, as will be shown below. Along the azimuthal angle of 15°, there are a set of stripes with a separation approximately  $\sqrt{2}$  times of that along 0° or 30°. Calibrated by the positions of Bragg stripes of graphene [ $2.949 \text{ Å}^{-1}$  and  $5.108 \text{ Å}^{-1}$  for graphene (01) and (11) peaks, respectively], the separation of stripes along each direction for SnSe are  $1.44 \pm 0.04 \text{ Å}^{-1}$  for (01),  $2.07 \pm 0.04 \text{ Å}^{-1}$  for (11), and  $1.46 \pm 0.04 \text{ Å}^{-1}$  for (10), which yield  $c = 4.36 \pm 0.12 \text{ Å}$  and  $b = 4.30 \pm 0.12 \text{ Å}$ . The ratio between the separations of (11) and (01) stripes,  $2.07/1.44 = 1.44$ , agrees well with the expected ratio of  $\sqrt{2}$ . Note that the lattice parameters determined from RHEED have relatively large errors. **c,d**, STM topography image (**c**) and simultaneously recorded  $dI/dV$  mapping image (**d**) of a large area with multiple SnSe plates. The numbers in **c** indicate the thickness of each plate in units of ML. Colored arrows in **d** indicate the six polarization directions of individual SnSe ML plates. Setpoints:  $V_s = -0.2 \text{ V}$ ,  $I_t = 5 \text{ pA}$ ,  $V_{\text{mod}} = 30 \text{ mV}$ . All resolvable polarizations in these ML plates are parallel to graphene's zigzag directions.

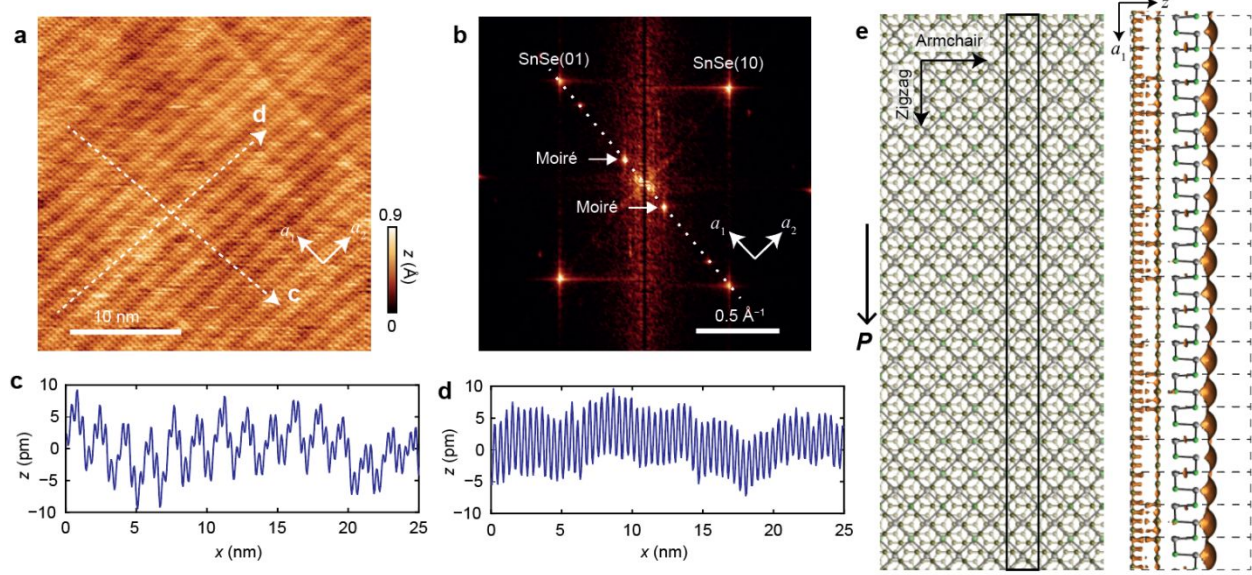


**Figure S2 | Moiré patterns resolved on the surface of a SnSe ML.** **a,b**, Atom resolved topographic image and its corresponding Fourier transform. Setpoints:  $V_s = -0.08$  V,  $I_t = 100$  pA. A stripe-shaped moiré pattern is generated from the overlapping of the SnSe ML and graphene lattices, and is also visible in Fourier transformed images. The SnSe(01) Bragg spots and the two spots from the moiré pattern fall on the same dotted line in **b**, implying moiré stripes perpendicular to the  $a_1$  axis of SnSe. The ratio  $R$  between the period of the moiré stripes and  $a_1$  is  $4.295 \pm 0.10$ , as seen in the apparent height profile extracted along the  $a_1$  axis of SnSe (**c**). On the contrary, the height profile along the  $a_2$  axis only shows an atomic corrugation (**d**). Although the atom-resolved images measured at room temperature are slightly distorted because of the inevitable sample drift induced by thermal fluctuations, we can extract relatively precise lattice parameters from moiré pattern simulations (Extended Data Figs. 3 and 4), given that the ratio  $R$  is not changed under a parallelogram distortion and that the lattice constant of graphene ( $a_g = 2.46$  Å) is known. **e**, Atomistic configuration of a SnSe ML on a graphene bilayer, obtained from first principles calculations. The darker (lighter) brown balls represent carbon atoms in the upper (lower) graphene monolayer. The rectangle indicates the supercell used in the calculation. The right panel shows the side view of the isodensity at  $-0.1$  eV below the Fermi energy for the SnSe ML on a commensurate bilayer graphene substrate. The fluctuation of the isodensity curve is consistent with the experimental moiré pattern. The Sn/Se atoms sit exactly at the middle line of two neighboring zigzag rows of graphene, consistent with a lattice matching scenario.



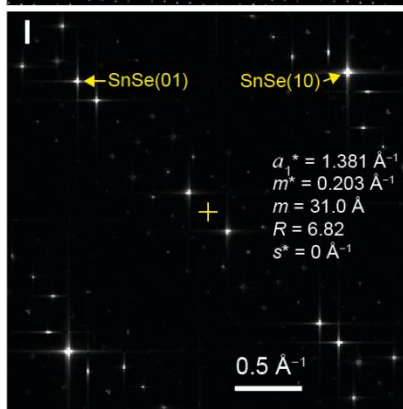
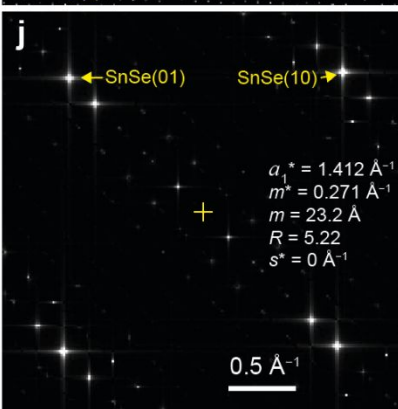
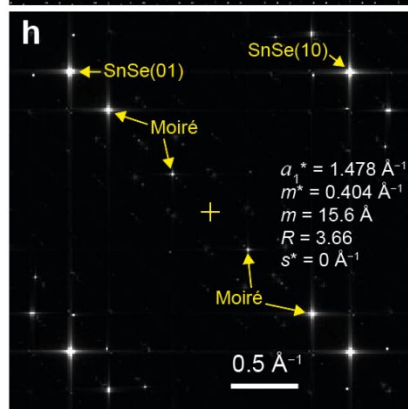
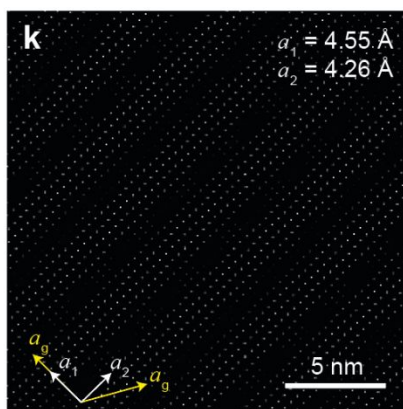
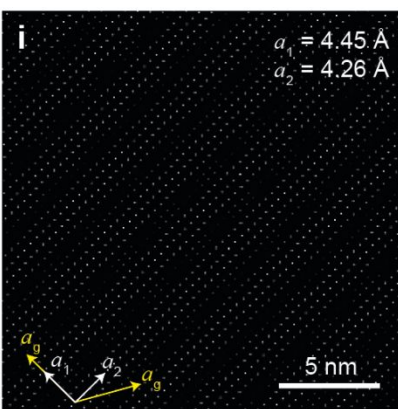
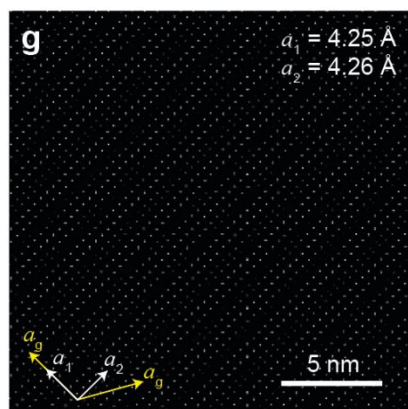
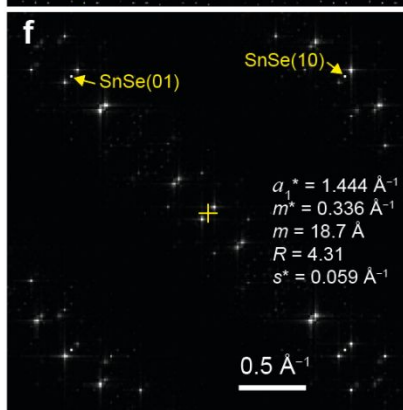
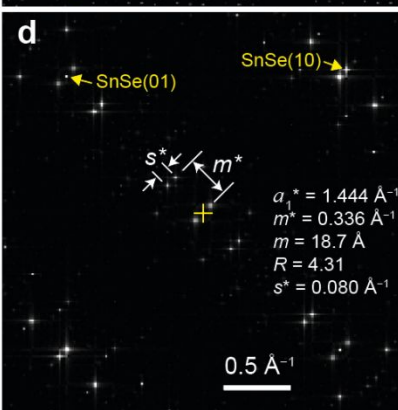
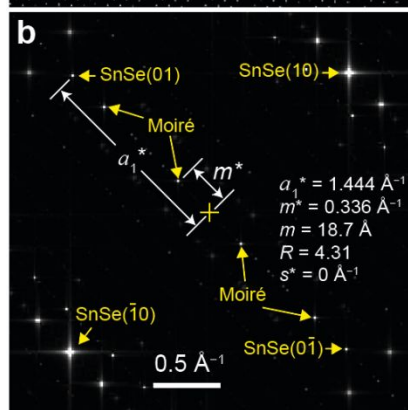
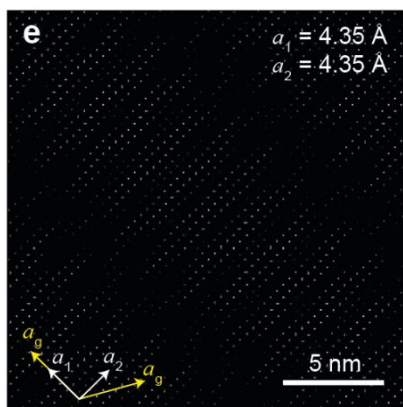
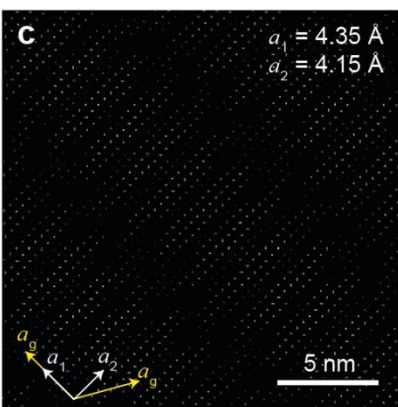
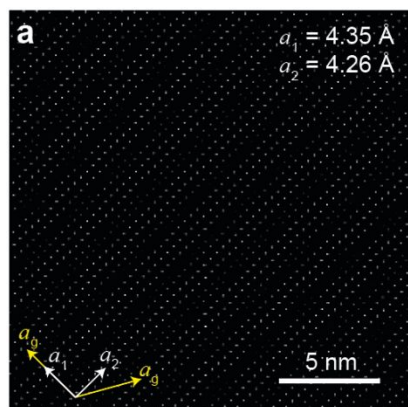


**Figure S3 | Simulated moiré patterns (a, c, e, h, i, k) and the corresponding Fourier transformed images (b, d, f, h, j, l).** The directions of lattice basis of graphene and SnSe are indicated by yellow and white arrows respectively in the real-space images. The zero point of each Fourier transformed image is labeled by a yellow cross. Quantities extracted from the Fourier transformed images are labeled in each panel:  $a_1^*$ , magnitude of the reciprocal base vector of  $\mathbf{a}_1$ ;  $m^*$ , magnitude of the reciprocal vector of moiré patterns;  $m$ , period of moiré stripes perpendicular to  $\mathbf{a}_1$ ;  $R$ , the moiré ratio defined as  $R = a_1^*/m^*$ ;  $s^*$ , distance between a pair of spots from moiré pattern. The definitions of  $a_1^*$ ,  $m^*$  and  $s^*$  are indicated in **b** and **d**. The moiré pattern that best agrees with experiment is shown in **a** and **b**; its SnSe ML lattice parameters are  $a_1 = 4.35 \text{ \AA}$  and  $a_2 = 4.26 \text{ \AA}$ . **c-f** are the images with values of  $a_2$  that are different from the one employed in **a**. For any values of  $a_2$  larger or smaller than  $4.26 \text{ \AA}$ , the moiré spots on the Fourier transform images will split by  $s^*$  (**d** and **f**). This can be understood from the lattice matching condition:  $\sqrt{3} \times 2.46 \text{ \AA} = 4.26 \text{ \AA}$ , in which  $2.46 \text{ \AA}$  is the lattice constant of graphene. Once  $a_2$  deviates from the commensurate value  $4.26 \text{ \AA}$ , a long-period beat pattern will generate between SnSe and graphene lattices along the  $\mathbf{a}_2$  direction (**c** and **e**); the period of this beat pattern is reflected by  $s^*$ . **g-l** show the moiré patterns calculated by fixing  $a_2$  at  $4.26 \text{ \AA}$  while changing  $a_1$ . In this case, the moiré spots show no splitting but the ratio  $R$  changes with  $a_1$ . In general,  $R$  has a monotonic dependence to  $a_1$  within the range of interest: a larger  $a_1$  leads to a smaller  $R$ .

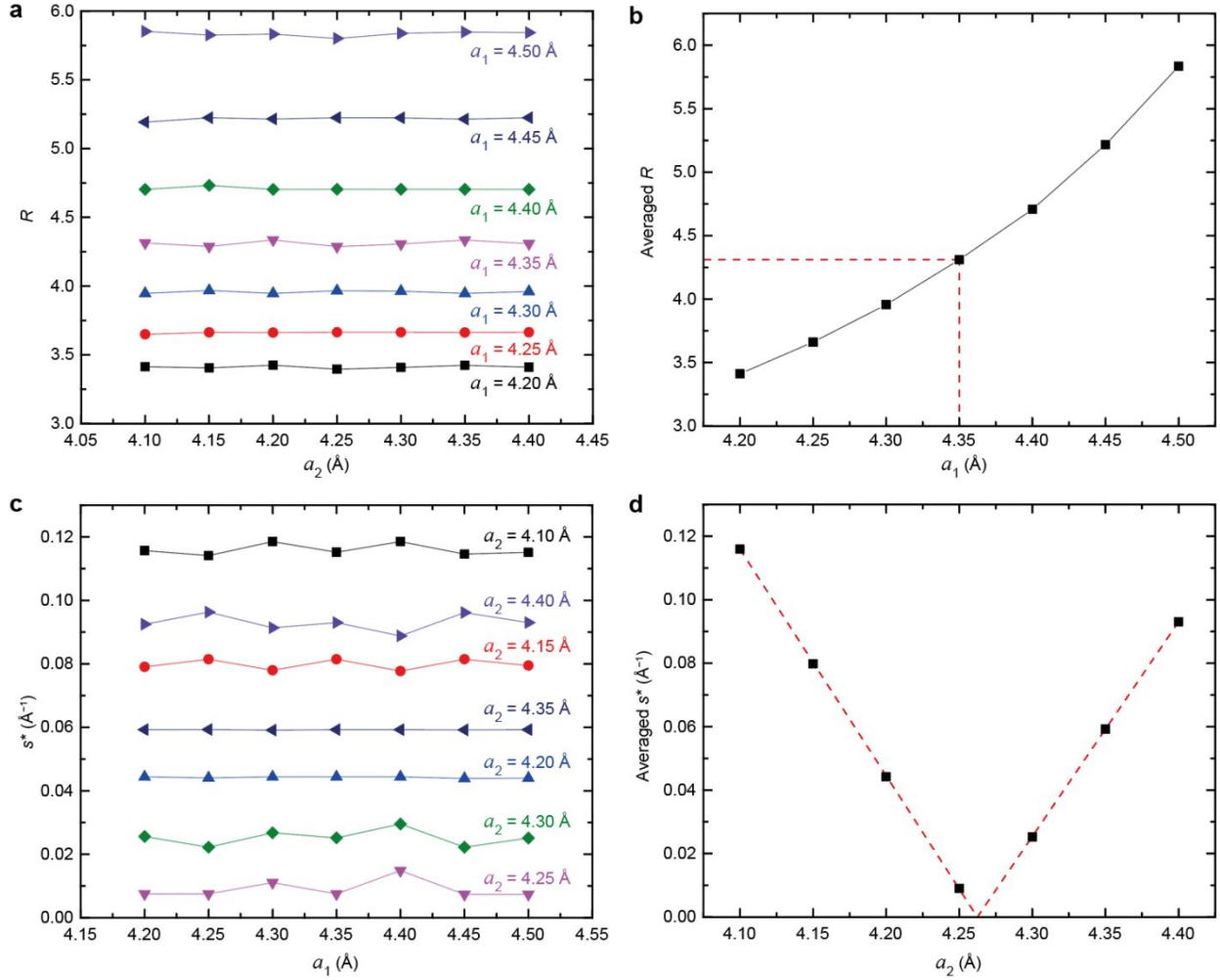


**Figure S4 | A systematic study of ratio  $R = a_1^*/m^*$  and splitting  $s^*$  extracted from simulated moiré patterns.** The crossing point of red dashed lines in **b** and **d** indicate the values that agree with the experiments. Within the error of the simulation, we found that the value of  $R$  is highly sensitive to  $a_1$  but is not influenced by  $a_2$ . On the other hand, the value of  $s^*$  is solely determined by  $a_2$ . Therefore, for such an orientation of basis vectors, the fittings of  $a_1$  and  $a_2$  can be decoupled. From the experimental values  $R = 4.295 \pm 0.10$  and  $s^* = 0$ , we can extract the lattice parameters  $a_1 = 4.35$  Å and  $a_2 = 4.26$  Å for monolayer SnSe, as the red dashed lines indicate in **b** and **d**.

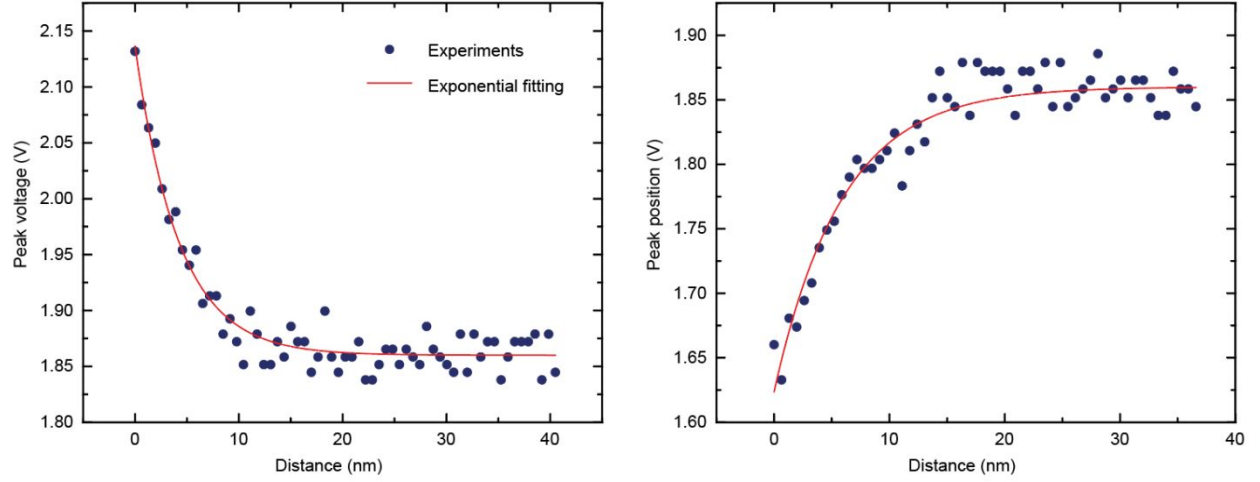


**Figure S5 | Fitting the band bending in Fig. 1c with an exponential decay function  $V(x) = A \exp [-(x - x_0)/L_0] + V_0$ .** The bending magnitudes  $A = +0.24$  V and  $-0.31$  V for upward and downward band bending respectively, are directly measured from the shape of VBM in Fig. 1c and thus used as fixed parameters in the fitting. The bias voltages corresponding to the LDOS peak at CBM,  $V_p(x)$ , are extracted by seeking the maximum values of the  $dI/dV$  spectrum at each position. In order to make sure that the fitted curves converge at the experimental value  $V_p(x \rightarrow \infty) = 1.86$  V (the averaged  $V_p$  at the band-bending-free areas of the nanoplate), we also fixed the voltage offset  $V_0$  at 1.86 V. The fittings yield  $L_0 = 4.22 \pm 0.23$  nm,  $x_0 = 0.59 \pm 0.13$  nm for upward bending, and  $L_0 = 5.89 \pm 0.36$  nm,  $x_0 = -1.60 \pm 0.32$  nm for downward bending. The decay length  $L_0$  is related to the strength of screening, while  $x_0$  is a parameter setting the position of the edge.

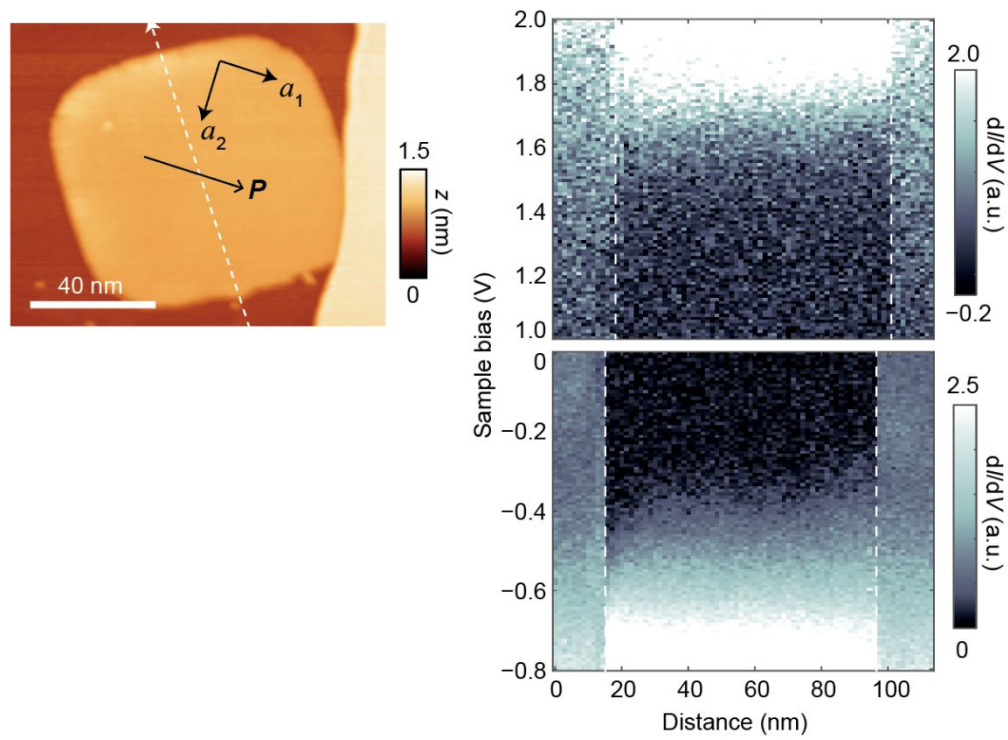


**Figure S6 | Spatially resolved  $dI/dV$  spectra acquired along the white dashed arrow across the SnSe ML plate shown in the left, obtained at room temperature.** Setpoints,  $V_s = 2.0$  V,  $I_t = 2$  pA for positive  $V_s$ ;  $V_s = -0.8$  V,  $I_t = 5$  pA for negative  $V_s$ . Finite band bending can still be resolved from the  $dI/dV$  spectra at room temperature.



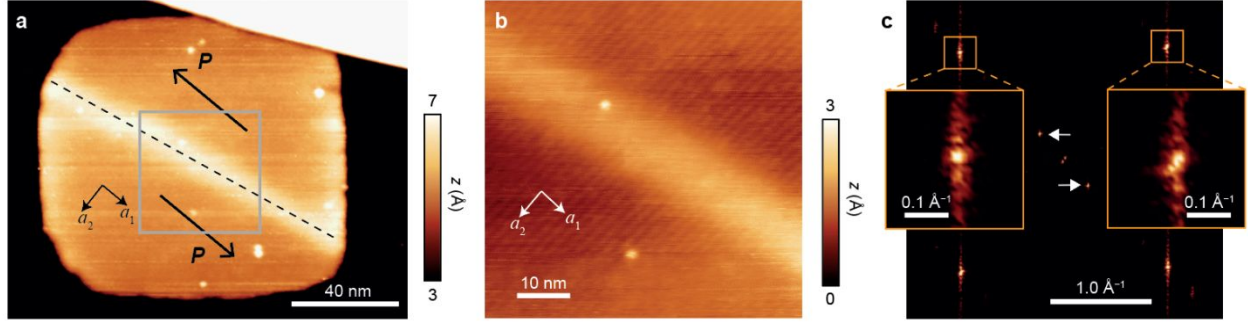


**Figure S7 | Atom resolved image across a 180° domain wall.** **a**, Simultaneously recorded topography image of the SnSe ML plate in Fig. 1f. The 180° domain wall is indicated by the dashed line. Setpoint:  $V_s = -0.2$  V,  $I_t = 2$  pA. **b**, Atom resolved topographic image across the 180° domain wall, acquired from the area labeled by the gray square in **a**. Setpoint:  $V_s = -0.2$  V,  $I_t = 100$  pA. **c**, Fourier transformed image of **b**. Insets are zoom-in images of the Bragg spots, which show no observable splitting. Arrows are spots from the moiré stripes. The absence of splitting in the Bragg spots implies identical lattice parameters in the two domains, in agreement with the lattice commensurate requirements of 180° domain walls.

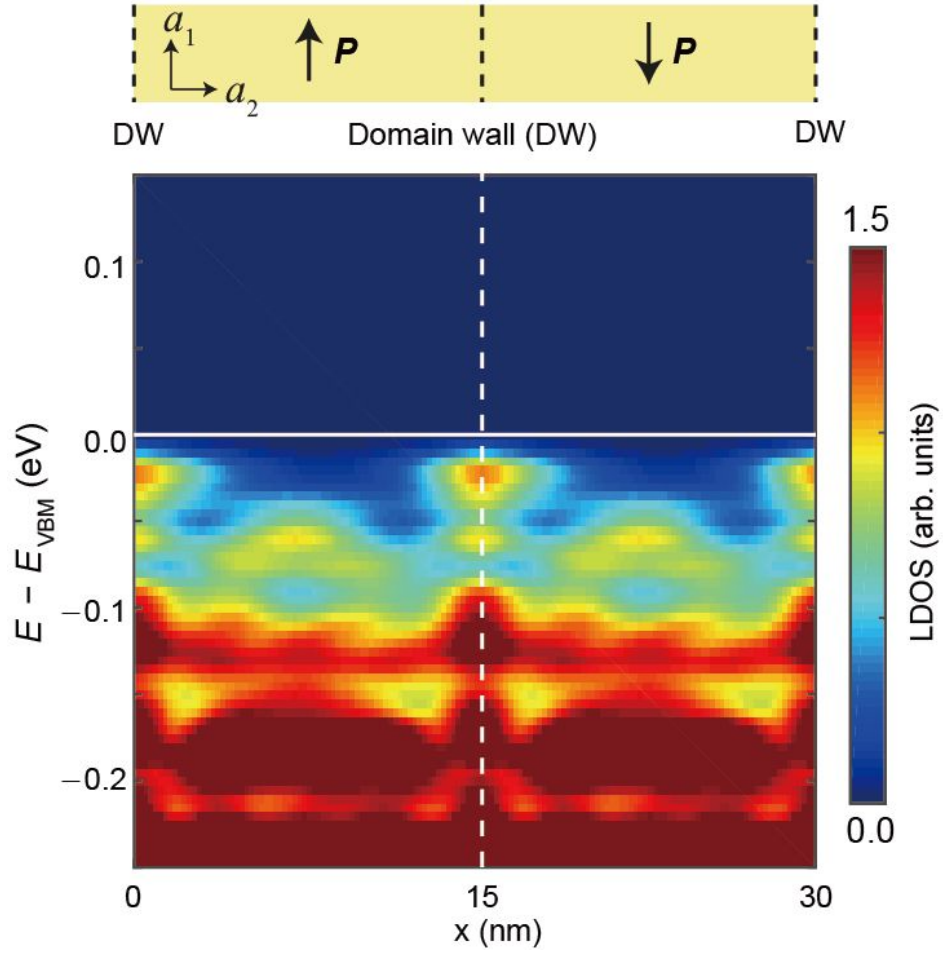


**Figure S8 | Spatial distribution of local density of states (LDOS) close to the valence band maximum in periodic 15-nm wide 180° domains, obtained from first principles calculation.** The domain walls are set to be strictly parallel with the polarization, thus neither bound charge nor band bending exists. Nevertheless, on the domain walls, a bound state at the VBM is revealed, which is responsible for the enhanced  $dI/dV$  intensity at the domain walls when the bias voltage is close to the VBM.

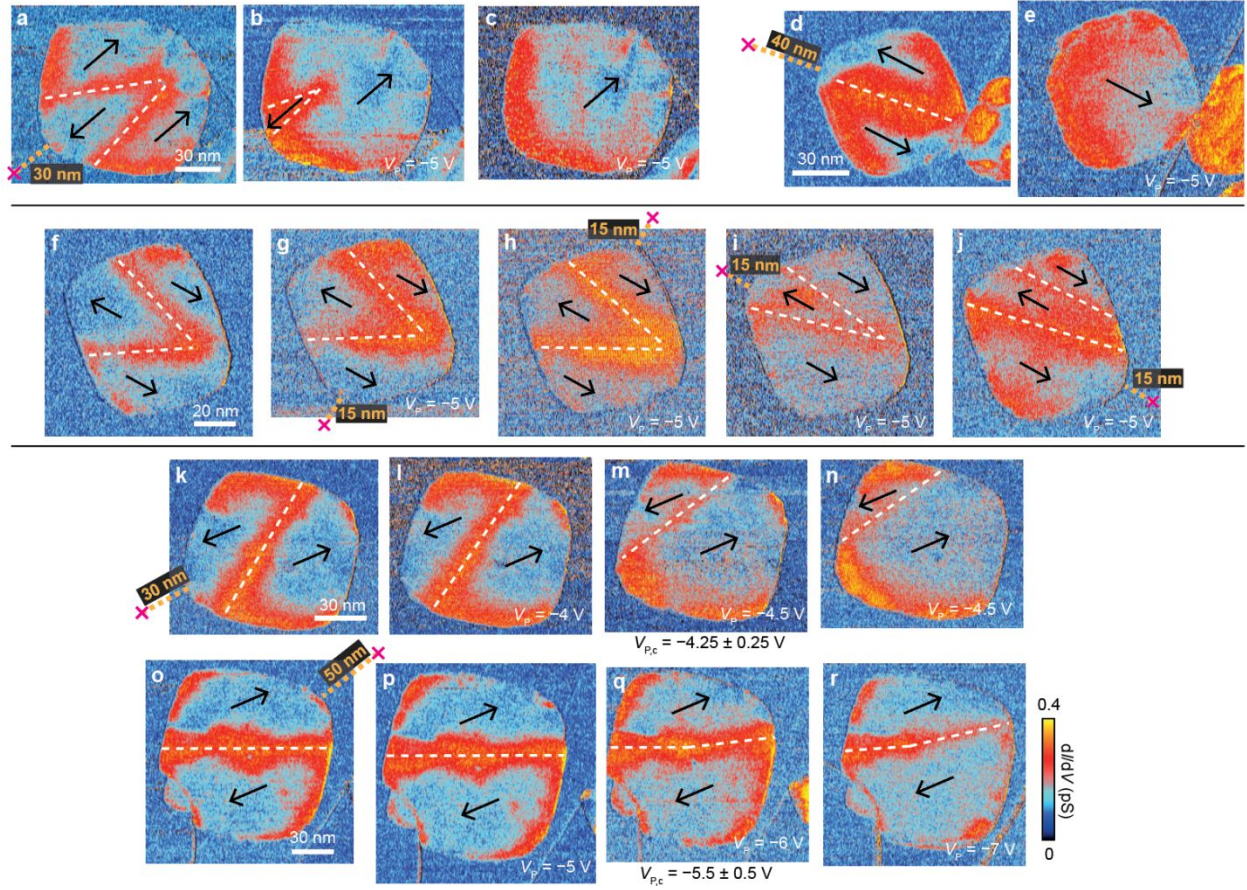


**Figure S9 | Ferroelectric switching experiments through domain wall motion in SnSe MLs.** **a-c** and **d-e** are two examples of setting multi-domain plates into single-domain with bias voltage pulses. The plate in **a-c** has a zigzag domain wall and the one in **d-e** has a straight wall. Domain walls are indicated by the white dashed lines. The positions where bias voltage pulses were applied are labeled by pink crosses. **f-j**, Pulses with the same  $V_P = -5$  V were applied near the four corners of a SnSe ML plate with a zigzag domain wall inside. The domain wall was moved only when the pulse was applied along a direction parallel to the polarization ( $a_1$  axis). **k-n** and **o-r** are two examples showing how critical pulse voltages  $V_{P,c}$  were measured with different  $d_0$ . For a certain plate, the position of pulses was always fixed. A relatively small  $V_P$  was applied at the beginning, and  $V_P$  was gradually increased until domain wall motion was observed. If the domain wall was not moved at  $V_{P1}$  but moved at  $V_{P2}$  after two consecutive pulses, then  $V_{P,c} = (V_{P1} + V_{P2})/2$  with an error bar ranging from  $V_{P1}$  to  $V_{P2}$ . Referring to the numerical simulations, we can convert  $V_{P,c}$  into the corresponding in-plane component of the electric field fields,  $E_{//}$ , as Fig. 3d shows. All the data were collected at room temperature. Setpoints:  $V_s = -0.35$  V,  $I_t = 2$  pA.

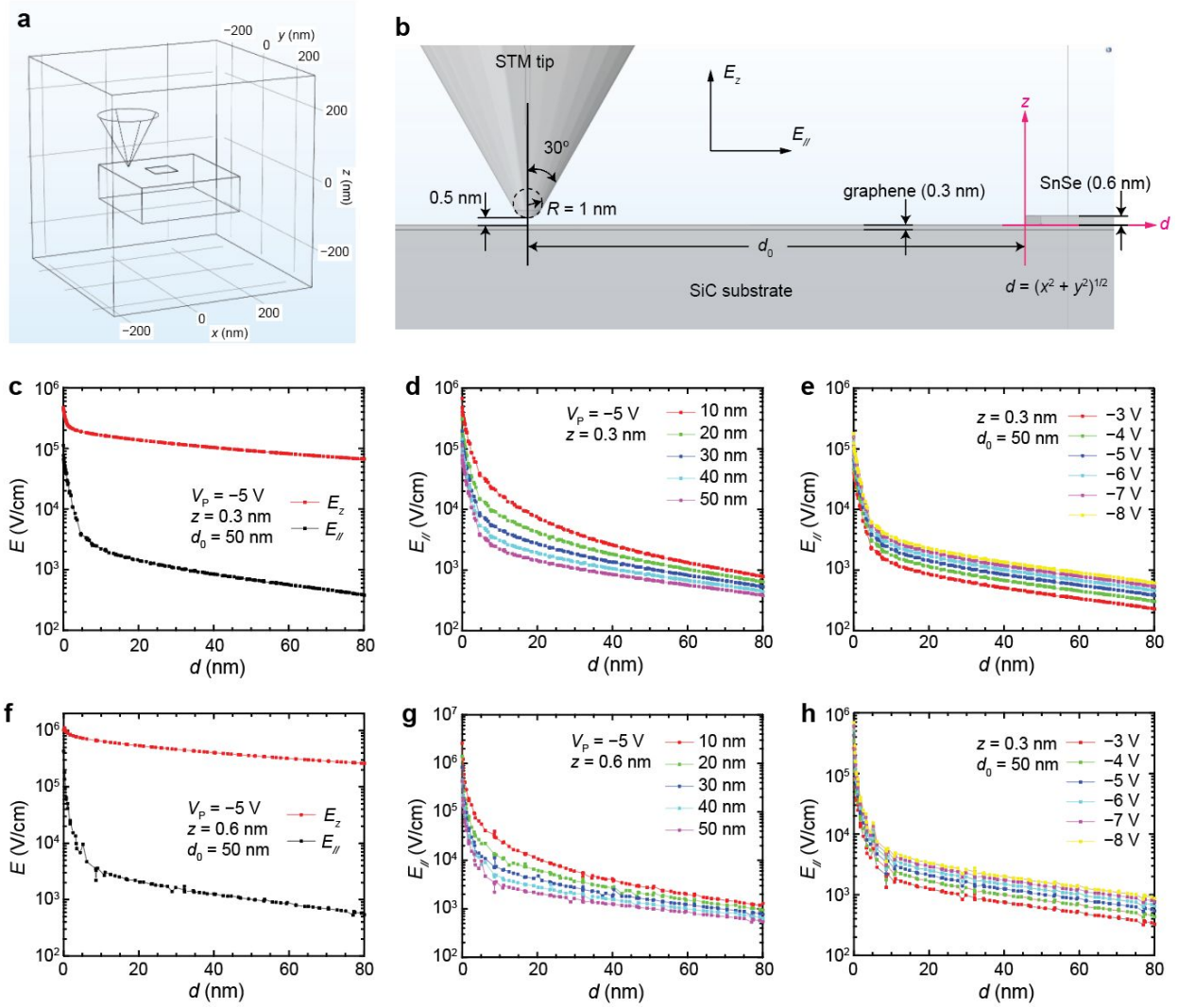


**Figure S10 | Details of the numerical simulation of bias voltage pulse induced electric field. a,b,** Illustrations of the model used for the simulation. The graphene layer was set as grounded, and a voltage of  $V_p$  was applied to the sample. The corner of SnSe closest to the STM tip was set as  $d = 0$ , and the upper surface of graphene was set as  $z = 0$ . **c,** Comparison between the out-of-plane and in-plane electric fields along a horizontal line along the  $d$  axis and at the height of  $z = 0.3$  nm, the middle line of SnSe. The other parameters are indicated in the panel. **d,** In-plane electric fields with  $V_p$  fixed while varying  $d_0$ . **e,** In plane electric fields with  $d_0$  fixed while varying  $V_p$ . **f-h,** Similar plots as **c-e**, but with  $z = 0.6$  nm, the upper surface of SnSe.



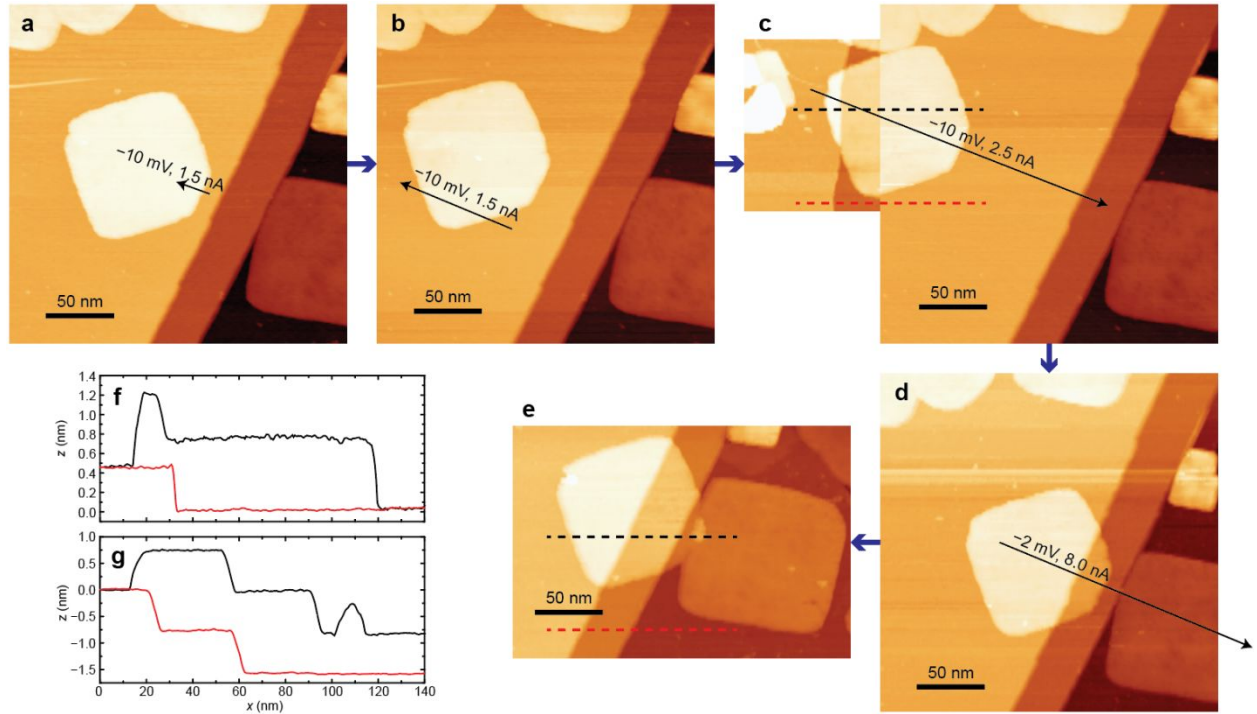


**Figure S11 | Controllably moving a SnSe ML plate by an STM tip.** a-e, Consecutively recorded topography images at room temperature. The SnSe ML plate was moved back and forth by moving the STM tip along the solid arrows with reduced tunneling barrier width. Specifically, the tip was first positioned at the starting point of an arrow with the setpoints of normal imaging ( $V_s = -0.4$  V,  $I_t = 2$  pA), then the tunneling conditions were set to the values indicated beside the arrow to “seize” the plate; the tip was moved along the arrow until reaching the ending point, and the tunneling conditions resumed the normal imaging setpoints to release the plate. The plate can be moved up (c) or down (d,e) the atomic steps on the substrate without damaging the plate itself, resembling of a carpet on stairs. The plate was blocked by another ML plate on its way and could not be moved further in panel e. f,g, Profiles of apparent height  $z$  extracted from the dashed lines in c (f) and e (g), respectively. The steps on the surface of the SnSe plate have exactly the same heights as those on the substrate underneath. The controlled motion of the SnSe ML plate suggests a van der Waals bonding between SnSe and the graphene substrate.